GLIA

GLIA 61:601–610 (2013)

Somatotopic Astrocytic Activity in the Somatosensory Cortex

ARKO GHOSH,[1,2,3]* MATTHIAS T. WYSS,[3,4] AND BRUNO WEBER[3,4]
[1]*Institute of Neuroinformatics, ETH and University of Zurich, Zurich, Switzerland*
[2]*Institute of Cognitive Neuroscience, University College London, London, United Kingdom*
[3]*Neuroscience Center Zurich, University of Zurich and ETH Zurich, Switzerland*
[4]*Institute of Pharmacology and Toxicology, University of Zurich, Zurich, Switzerland*

KEY WORDS
astrocyte; somatotopy; forelimb; hindlimb; electrical stimulation; fluoroacetate; neuroglial communication; tetrodotoxin

ABSTRACT
Astrocytes play a crucial role in maintaining neuronal function and monitoring their activity. According to neuronal activity maps, the body is represented topographically in the somatosensory cortex. In rats, neighboring cortical areas receive forelimb (FL) and hindlimb (HL) sensory inputs. Whether astrocytic activity is also restricted to the cortical area receiving the respective peripheral sensory inputs is not known. Using wide field optical imaging we measured changes in the concentration of astrocytic calcium within the FL and HL sensorimotor cortex in response to peripheral sensory inputs. Mapping the calcium signals upon electrical stimulation of the forepaw and hindpaw we found activity largely restricted to the FL and HL area, respectively. In comparison to neuronal activity the time course of the astrocytic calcium activity was considerably slower. The signal took 6 s to peak after the onset of a 2 Hz and 2 s long electrical stimulation of the hindpaw and 8 s for a 4 s stimulation. The astrocytic signals were delayed relative to cerebral blood flow measured using laser speckle imaging. The intensity of both the astrocytic and neuronal signals in the HL sensorimotor cortex declined with increase in stimulation frequency. Moreover, blocking neuronal input by tetrodotoxin abolished astrocytic calcium signals. We suggest that the topographical representation of the body is not only true for cortical neurons but also for astrocytes. The maps and the frequency-dependent activations reflect strong reciprocal neuroglial communication and provide a new experimental approach to explore the role of astrocytes in health and disease.

INTRODUCTION

Astrocytes are essential for brain function and they house the mechanisms to nourish neurons (Pellerin and Magistretti, 1994), regulate neurotransmitter release (Kozlov et al., 2006; Perea and Araque, 2007) and modulate neuronal plasticity (Pascual et al., 2005). Intracellular calcium is important for signaling within astrocytes and it is elevated in response to enhanced neuronal activity (Aguado et al., 2002). Calcium waves typically spread through gap junctions in the astrocytic network (Giaume et al., 2010) and importantly, drive the release of gliotransmitters to influence neuronal activity (Mothet et al., 2005; Navarrete et al., in press). Nevertheless the spatial extent of these waves is contentious; the waves propagate to a much larger extent in cell culture monolayers than in brain slices (Cornell-Bell and Finkbeiner 1991; Nett et al., 2002). Recent studies using two-photon microscopy to measure calcium signals *in vivo* have revealed how single astrocytes participate in neurovascular coupling (Takano et al., 2006; Iadecola and Nedergaard 2007) and the orientation tuning of astrocytes in the visual system (Schummers et al., 2008). Interestingly, increases in intracellular calcium have been observed in response to somatosensory inputs (Wang et al., 2006; Winship et al., 2007). The somatotopic representation of the body in cortical neurons has been conveyed in detail, but how does it relate to the spatial distribution of astrocytic activity? In particular, does the neuronal activity elicited by the activation of a specific body part result in astrocytic calcium elevation in the corresponding cortical area? As astrocytes are closely associated with neuronal synapses (Araque and Navarrete, 2010) somatotopy must exist in the glial cells, unless their gap junctions propagate the signals to the noncorresponding cortical areas.

Astrocytic calcium increases are closely associated with hemodynamic changes (Zonta et al., 2003; Takano et al., 2006) which instead is used as a proxy for neuronal activity. Interestingly, blood flow-related changes mostly measured using BOLD-fMRI, intrinsic or laser speckle imaging reveal separate forelimb (FL) and hindlimb (HL) representations in the somatosensory cortex (Dunn et al., 2005; Sydekum et al., 2009). The hemodynamic maps correspond well to neuronal activity detected using single or multiunit recordings and voltage sensitive dye optical imaging (Gochin et al., 1992; Ghosh et al., 2009; Sydekum et al., 2009). The area activated by forepaw electrical stimulation lies rostral to the

Arko Ghosh and Matthias T. Wyss contributed equally to this work.

Grant sponsor: Swiss National Foundation; Grant number: 31003A-124739/1, PP0033-110751; Grant sponsor: Society in Science-The Branco Weiss Fellowship; Grant sponsor: European Union funded SECO; Grant number: 216593; Grant sponsor: Human Frontier Science Program; Grant number: RGP0032/2010.

*Correspondence to: Arko Ghosh, Institute of Neuroinformatics, ETH and University of Zurich, Winterthurerstr. 190, CH-8057, Zurich, Switzerland. E-mail: arko@ini.phys.ethz.ch

Received 13 February 2012; Accepted 5 December 2012

DOI 10.1002/glia.22458

Published online 22 January 2013 in Wiley Online Library (wileyonlinelibrary.com).

HL cortex (Sydekum et al., 2009). As the neurovascular interactions underlying these signals are in part mediated by astrocytes (Iadecola and Nedergaard, 2007) neuronal and astrocytic maps too should be overlapping.

FL and HL sensory areas have a neuron-packed granular layer IV and they receive their inputs relayed via the somatotopically organized sensory thalamus (Zilles et al., 1980; Francis et al., 2008). Although the anatomy of the astrocytic network in these areas is not known, the intercellular connectivity of astrocytes in the adjacent whisker cortex is largely restricted within individual barrels (Houades et al., 2008). It must be stated here that apart from the strong dominance of FL input to the neurons in the corresponding cortical area, an attenuated version of the same input is fed to the HL area (Ghosh et al., 2010).

To reveal the spatiotemporal dynamics of astrocytic calcium in the somatosensory cortex, we focused on the FL and HL representations of rats. We measured the changes in intracellular calcium levels using the fluorescent indicator Rhod-2 AM and widefield optical imaging in the sensorimotor cortex. Similar to neuronal activity and blood flow, the astrocytic responses to forepaw and hindpaw electrical stimulation were mostly restricted to the corresponding cortical areas. Thus, in response to peripheral inputs, neuronal activity in one cortical area has only marginal influence on the astrocytic activity of remote areas, and the body is also represented somatotopically in astrocytes.

MATERIALS AND METHODS

Animals

The experiments were carried out by licensed investigators and were approved by the local veterinary authorities. In total, 27 animals (female Lewis rats weighing 200–300 g) were included in the study. Prior to the experiments, the animals were housed in cages in a ventilated cabinet with standardized conditions of light (night/day cycle: 12/12 h) and temperature. Free access to food and water was always ensured.

Surgical Preparation

All the surgical procedures were performed under isoflurane anesthesia (2.5–3.5% in air/oxygen 70/30%) and involved the placement of vessel catheters (PE-50) into the right femoral artery and vein and tracheotomy for artificial ventilation. Vessel catheters were used for continuous blood pressure monitoring (artery) and administration of physiological saline solution at regular intervals to maintain volume homeostasis (vein). In addition, blood samples were regularly withdrawn for arterial blood gas analysis. For optical widefield imaging experiments, a craniotomy was performed above the somatosensory cortex [bregma, 2 to −5 mm; lateral, 2–7 mm (Paxinos and Watson, 2006)] using a dental drill to expose the dura. Before staining, the dura was carefully removed and the bregma was marked using a blue ink visible to the imaging set up. Dental cement was used to build a well to prevent dye leakage during the staining process. The actual experiments were performed under α-chloralose anesthesia (44 mg/kg body weight s.c.) according to the protocol of Bonvento et al. (1994). The temperature of the animals was kept at 37°C with a heating blanket and blood gases were maintained within physiological ranges by adjusting the ventilation when necessary. At the end of each experiment, animals were sacrificed using an intravenous lethal dose of pentobarbital.

Sensory Stimulation

The forepaw and hindpaw contralateral to the imaged hemisphere were stimulated following a baseline of 2 s, using a four- or eight-pulse train, with 800 μA currents. Only one paw was stimulated at a time and the pulses were 1 ms long separated by 499 ms (2 Hz). In experiments testing for frequency-dependence gaps between individual pulses varied between 49 (20 Hz) and 499 ms (2 Hz). For all intrinsic and laser speckle imaging measurements eight pulses were used. In voltage-sensitive dye (VSD) imaging experiments 1 ms long pulses were applied after a baseline of 100 ms.

Pharmacoloical Interventions

Fluoroacetate (FA; 100 M) was topically applied during four Rhod-2 experiments, three VSD measurements, three intrinsic imaging experiments, and four electrophysiological recordings. FA is a specific astrocytic toxin that blocks the tricarboxylic acid cycle (Fonnum et al., 1997). After 100 min of incubation, the cortex was washed with Ringer's solution (NaCl 8.6, $CaCl_2$ 0.33, KCl 0.30 g/L).

In addition, during four Rhod-2 and three electrophysiological measurements, 20 μM tetrodotoxin (TTX) was topically applied for 60 min.

Intrinsic Optical, Laser Speckle, and Rhod-2 Imaging

These three imaging modalities were applied in succession in the same field of view in the same animal. Cortical images were acquired using a 12-bit CCD camera (Pixelfly VGA, PCO Imaging, Kelheim, Germany) attached to a motorized epifluorescence stereomicroscope (Leica MZ16 FA, Leica Microsystems, Heerbrugg, Switzerland) focused 0.5 mm below the cortical surface. For intrinsic optical imaging, the wavelength was fixed at 570 nm (10 nm FWHM) produced with a monochromator (Polychrome V, Till Photonics, Grafelfing, Germany) and coupled to the microscope using an optical fiber. At 570 nm, deoxyenated and oxygenated hemoglobin demonstrate a so-called isosbestic point, and consequently the signal closely reflects total hemoglobin changes. Images were acquired at 30 Hz.

Laser speckle imaging was employed to measure cerebral blood flow (CBF). The method is described in detail

elsewhere (Zakharov et al., 2009). A 785 nm laser (TuiOptics, Munich, Germany) was used to acquire images at 50 Hz with an exposure time to 10 ms.

For Rhod-2 imaging, the cell-permeant acetoxymethyl ester form of Rhod-2 (250 g mixed in 10 L dimethyl sulfoxide and 190 L calcium free Ringer's solution, Rhod-2 AM, Invitrogen AG, Basel, Switzerland) was used to stain the somatosensory cortex for 90 min. The incubation was followed by a wash with dye-free Ringer's solution for 15 min. Afterwards, the fluid-filled chamber was covered with a glass coverslip. Rhod-2 AM was excited at 570 nm using the same monochromator and emitted light was collected after passing through a 590 nm longpass filter (Carl Zeiss AG, Göttingen, Germany). Images were acquired at 20 Hz. To control for depth penetration of the dye, in two animals, directly after imaging studies, brains were removed, frozen in chilled isopentane and sectioned (50 μm coronal slices). Rhod-2 AM fluorescence was then acquired with a camera mounted on a confocal fluorescence microscope.

VSD Imaging

For VSD imaging, the dye RH1691 (Optical Imaging, Rehovot, Israel) was dissolved at 1 mg/ml in Ringer's solution. The dye was topically applied and was allowed to diffuse into the cortex for 90 min. During staining, the dye was continuously circulated by a peristaltic pump (Reglo digital, Ismatec SA, Glattbrugg, Switzerland). Thereafter, the unbound dye was removed and the area was washed with dye-free Ringer's solution for 15 min. The fluid-filled chamber was then covered with a glass coverslip. For imaging, the dye was excited with 630 nm light from a LED lamp (Thorlabs GmbH, Dachau/Munich, Germany). The excitation light was reflected by a 650 nm dichroic mirror and focused onto the cortical surface with a camera lens. Fluorescent emission light was collected via the same optical pathway, but without mirror reflection, longpass filtered (>670 nm) and focused onto the sensor of a high-speed Micam Ultima camera (Scimedia, Costa Mesa, CA). Images were collected with 1 ms temporal resolution. In VSD experiments, three animals were examined without FA, while three animals were examined before and after topical application of FA.

Two-Photon Microscopy

For two-photon microscopy, the cortex was stained with Rhod-2 AM as described above. Two-photon microscopy was performed using a custom-built microscope with a ×40 water immersion objective (NA 0.8, Olympus, Japan). Rhod-2 was excited at 870 nm (150 fs pulse width) with a titanium sapphire laser. For scan mirror control and photomultiplier data acquisition, Helioscan software was used (Langer et al., 2010). Anatomical imaging was performed at a resolution of 256 × 256 pixels with averaging over five frames.

Electrophysiology

A Neuronexus probe was slowly inserted 3–600 μm deep to target the superficial cortical layers. Signals were amplified using a 1,000× gain and digitized using a two-step amplifier (Multi Channel Systems, Reutlingen, Germany). A 2 s baseline period was collected prior to each stimuli train.

Data Analysis

Image analysis was performed using custom-written Matlab routines and the software package PMOD (PMOD Technologies, Adliswil, Switzerland). Ten trials were averaged for each subexperiment for all imaging modalities.

Intrinsic optical imaging: The magnitude of intrinsic signals was calculated as the fractional change in reflected light intensity relative to prestimulus baseline.

Laser speckle imaging: To quantify CBF, speckle images were processed using 5 × 5 spatial and 25 temporal binning [for further details see Zakharov et al., (2009)].

Rhod-2 imaging: Rhod-2 data were acquired from the same field of view as in intrinsic imaging. Calcium increases were measured as relative increases of fluorescence from the baseline intensity ($\Delta f/f_0$).

For all optical imaging modalities (intrinsic optical, laser speckle and Rhod-2 imaging) ROIs were derived from 50% isocentric contours at the time of maximal response.

VSD imaging: Time courses of fluorescence changes were quantified as $\Delta f/f_0$ from ROIs using 50% isocentric contours drawn at peak response. Amplitude was defined as the difference between the maximal response and the baseline signal just before the onset of paw stimulation. Bleaching of fluorescence was corrected by subtraction of a best-fit double exponential.

Electrophysiology: The data was band-pass filtered between 200 and 15,000 Hz to reveal multiunit activity. Spikes were detected using a 3.4 standard deviation threshold. Z-scores are based on stimuli triggered analysis conducted using Neuroexplorer (Nex Technologies, Littleton, MA).

Statistics

Data sets consisting of more than two groups were first evaluated using nonparametric ANOVA for multiple comparisons followed by the Mann–Whitney U Test. When only two groups were compared, the Mann–Whitney U test alone was used. The threshold for statistical significance was set at $P < 0.05$ in all the tests.

RESULTS

Astrocytic Staining with the Calcium-Sensitive Dye Rhod-2 AM

When the dye Rhod-2 is applied topically (on the cortex; Fig. 1A), as in this study, it is known to selectively

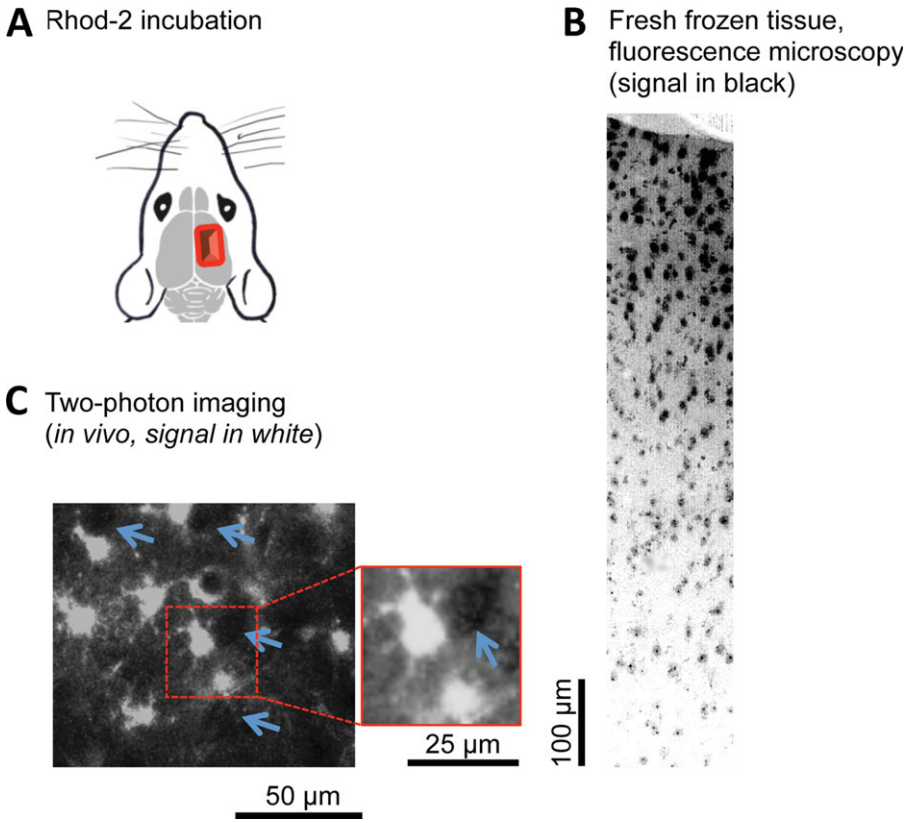

Fig. 1. Astrocytes labeled with Rhod-2 AM for widefield imaging. (**A**) The rat somatosensory cortex was bathed in a solution containing Rhod-2 AM. (**B**) Astrocytes were strongly labeled in the superficial 200 µm of the cortex as revealed in fresh frozen brain sections. (**C**) Two-photon imaging of the living brain revealed loaded astrocytes with unfilled structures (blue arrows), presumably neurons. Note a blood vessel surrounded by astrocytic endfeet (center of the image).

label astrocytes (Wang et al., 2006). Employing two-photon imaging *in vivo* and fluorescence microscopy of frozen brain sections, we were able to qualitatively assess the specific uptake of Rhod-2 AM by astrocytes. Notably, the widefield imaging method used here is expected to detect the calcium signals originating mostly from 1 to 200 µm deep astrocytes. According to frozen brain sections, Rhod-2-labeled cells were visible even at 1 mm, albeit the intensity is dramatically reduced below 200 µm (Fig. 1B). *In vivo* two-photon imaging revealed "star-shaped" Rhod-2-filled cells and amidst them were unfilled cells—presumably neurons (Fig. 1C). We did not observe any filled structures typical of neurons, such as the dendritic trunk or basal dendrites of pyramidal neurons.

Verification of the Astrocytic Origin of the Calcium Signals

The Rhod-2 (calcium) signals and peripheral electrical stimulation of the FL and HL revealed distinct representations in the contralateral somatosensory cortex (Fig. 2A). We also measured intrinsic optical signals—without the dye—and this revealed similar representations (Fig. 2B). Previous studies using topically applied calcium indicators including Rhod-2 (Mulligan and MacVicar 2004; Takano et al., 2006; Wang et al., 2006) and our own anatomical observations mentioned above lead us to believe that the signals are of astrocytic origin. We further confirmed this by blocking astrocytes using FA (Fig. 2A), which led to elimination of the Rhod-2 signal. Similarly, the hemodynamic signal obtained during repeated stimulation using intrinsic optical imaging was abolished after FA application (Fig. 2B). The calcium signal visible before the block was completely abolished (for 2 s long HL stim: before FA mean peak 0.85% $\Delta f/f_0$ ± 0.02 SEM and afterwards −0.01% $\Delta f/f_0$ ± 0.04 SEM, $n = 4$, $P < 0.05$). This difference in the imaged calcium and neuronal activity demonstrates that the imaging method does not detect neuronal calcium changes and that the signals are of astrocytic origin. An early negative dip in the signal was clearly visible, *albeit* more prominently in the absence of astrocytic activity (i.e., in the presence of FA, Fig. 2C,D). We think this early Rhod-2 signal is affected by hemodynamic changes (increased absorption due to increased blood volume). However, their contribution to the much larger positive Rhod-2 signal is only marginal. Notably, the blocker did not prevent neuronal activity in the somatosensory cortex. According to the electrophysiological recordings, neurons were more responsive to hindpaw stimulation after FA (mean increase in z-score peak of 70% ± 30 SEM, $n = 4$, Fig. 2E,F).

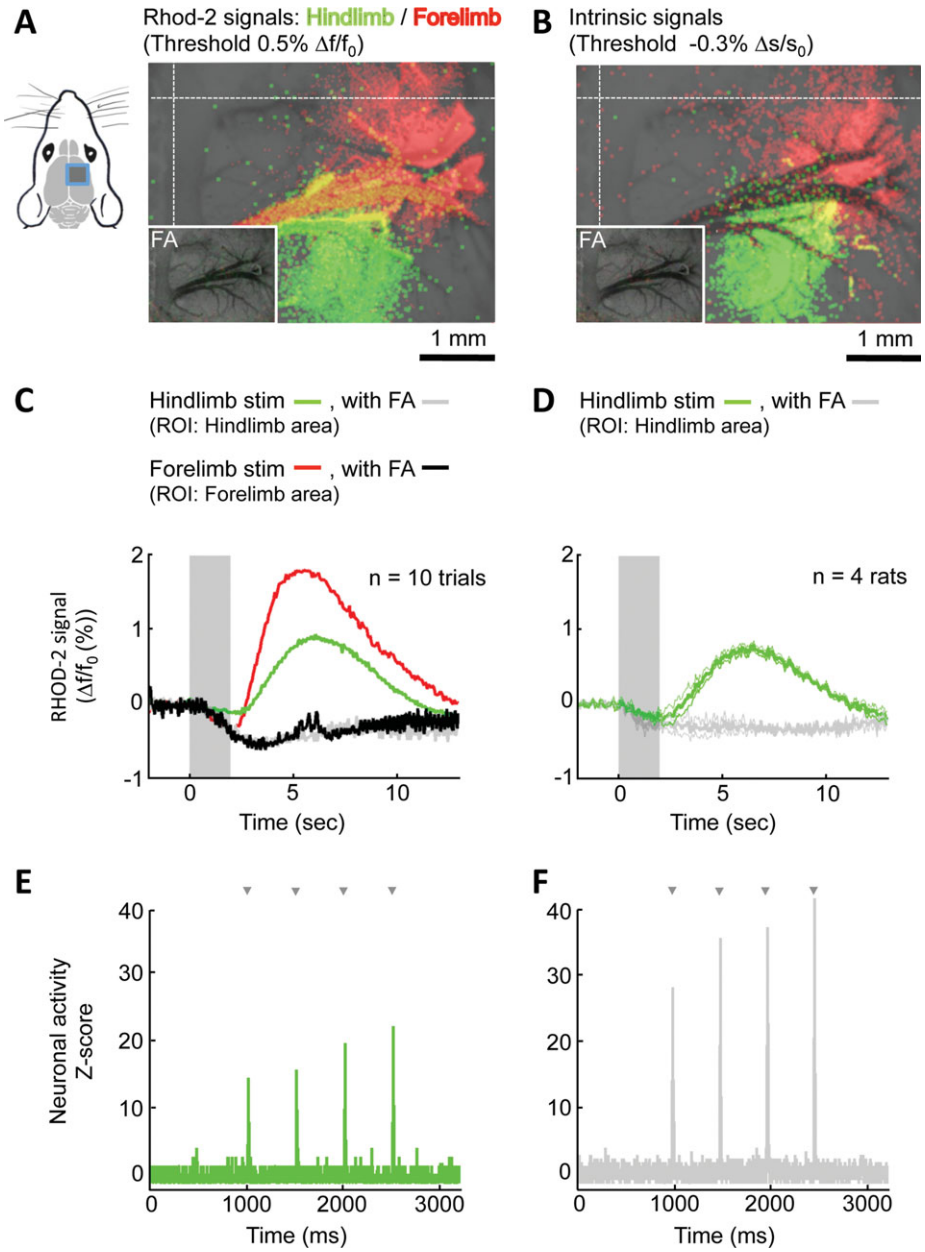

Fig. 2. Widefield imaging of astrocytic calcium signals following contralateral FL and HL electrical stimulation. (**A**) Upon 2 s stimulation at 2 Hz (four pulses) the Rhod-2 AM signal revealed clearly separated FL and HL astrocytic maps (6 s post-stimulus onset). Dashed lines meet at the bregma. (**B**) Intrinsic signals averaged in the same animal revealed the FL and HL sensory areas. Maps obtained after stimulations of the FL and HL (10 trials each, eight 1 ms long pulses, interval of 499 ms, 800 μA current). The inserts in (A) and (B) show the corresponding signal after 100 min of fluoroacetate (FA) incubation. (**C**) Time courses of the astrocytic activity in the presence and absence of FA in one animal. (**D**) Grouped data from four animals after HL stimulation with and without FA. Thin lines show the data ± SEM. In (C) and (D), 50% isocentric contours were used as ROIs. The shaded area (in gray) indicates the duration of the stimulation. Note the absence of positive fluorescence signal in the presence of FA. Multiunit neuronal activity of a single animal before (**E**) and after application of FA (**F**), gray arrows mark the time of stimulation (same as above, but the first four responses in each stimulation train were analyzed).

Comparison of Astrocytic Calcium Signals, CBF Responses and Neuronal Activity

We used three different imaging techniques to put the astrocytic signals in context to neuronal and blood flow changes. The astrocytic Rhod-2 signals were clearly visible 4 s after HL or FL stimulus onset (time to peak for 4 s long stimulation (2 Hz): HL 8.9 s ± 0.5 SEM and FL 7.9 s ± 0.3 SEM, $n = 4$, $P < 0.05$, Fig. 3A,B,B′). The signals upon HL stimulation originated from an area that was located caudo-medial to the FL sensory area (Fig. 3A). These sites of origin were continuously recruited at later time points until the signal faded. The amplitude in response to HL stimulation was lower than the

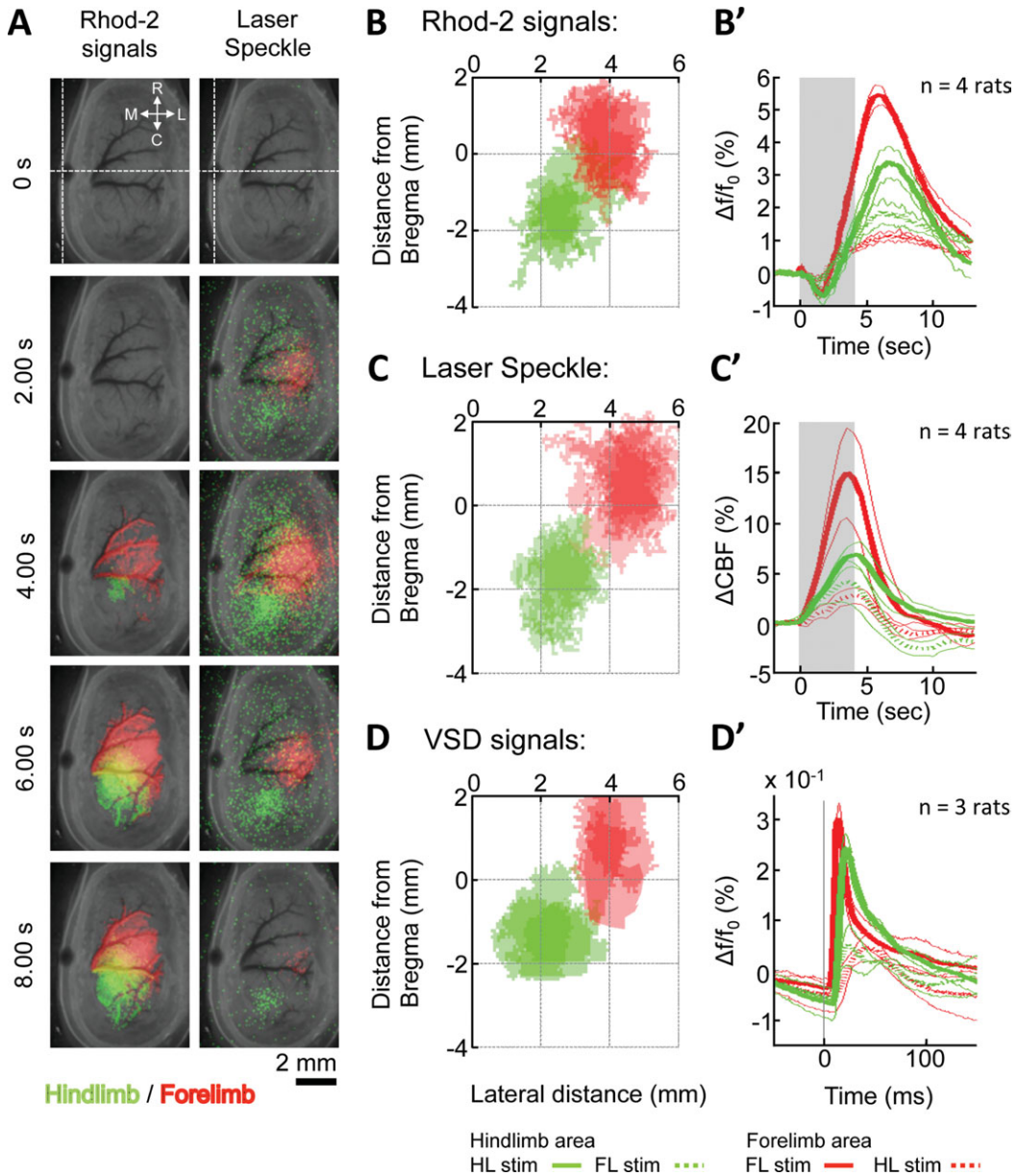

Fig. 3. Astrocytic calcium maps overlap with evoked cerebral blood flow (CBF) signals and neuronal activity. (**A**) Spatiotemporal dynamics of astrocytic calcium activity in the two respective areas (on the left) in comparison to the CBF signal (on the right). Dashed lines meet at the bregma. Mapping of astrocytic Ca^{2+} signals (**B**), CBF (**C**, laser speckle imaging) and neuronal activity (**D**, VSD imaging) in a coordinate system reveals the high spatial consistency of three different read-outs. (B′)–(D′) Correspondig time course of the three modalities. Thin lines show the data ± SEM. 50% isocentric contours were used as ROIs. The shaded area (gray) indicates the duration of the stimulation.

response upon FL stimulation (HL area: mean response amplitude to HL stimulation: 3.4% $\Delta f/f_0$ ± 0.6 SEM; FL area: mean response amplitude to FL stimulation: 5.4% $\Delta f/f_0$ ± 0.4 SEM, $n = 4$, $P < 0.05$, Fig. 3B′).

Using the same stimulation paradigm, laser speckle imaging revealed a surprisingly quicker change in blood flow compared with the detected astrocytic signals. It was visible within 2 s of stimulus onset (latency to peak for 4 s long stimulation (2 Hz): HL 6.1 s ± 1.5 SEM and FL 5.5 s ± 1.5 SEM, $n = 4$, $P < 0.05$, Fig. 3C′). As for the astrocytes, we compared the HL and FL amplitudes and found a stronger activation by the latter (peak amplitude HL 6.7% ΔCBF ± 1.1 SEM and FL 14% ΔCBF ± 5.5 SEM, $n = 4$, $P < 0.05$, Fig. 3C′). Although blood flow and astrocytic maps (both based on peak activations) occupied overlapping territories (Fig. 3A–C), the regions near surface veins provided a significant source of Rhod-2 signals.

Neuronal imaging with voltage sensitive dye revealed the same HL and FL representations (Fig. 3D). As expected, the neuronal signals were the quickest of the three measures and visible within 12 ms of stimulus onset (time to peak upon a 1 ms long pulse to HL 22 ms ± 3 SEM and to FL 14 ms ± 3 SEM, $n = 4$, $P < 0.05$

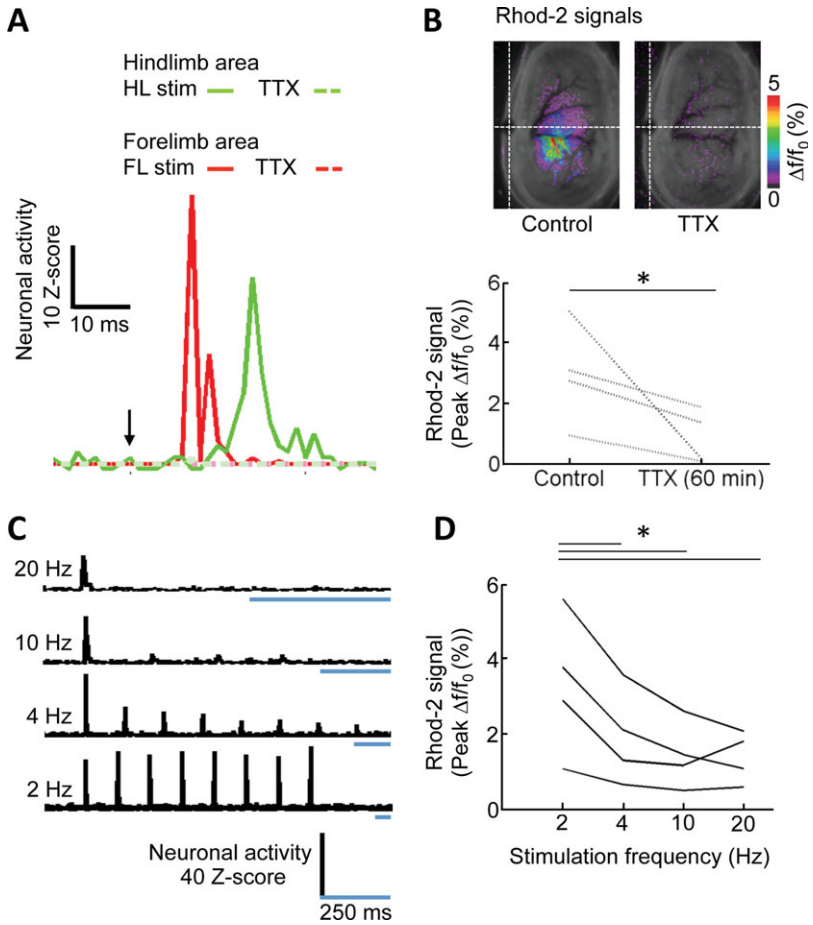

Fig. 4. Astrocytes are highly dependent on neuronal input. Application of TTX abolishes neuronal activity according to multiunit recordings (**A**). (**B**) In parallel, astrocytic Rhod-2 signals are heavily diminished ($n = 4$, * = $P < 0.05$). (**C**) With increasing stimulation frequency (from 2 to 20 Hz) neuronal responses (C) and astrocytic calcium activities (**D**) decrease ($n = 4$, * = $P < 0.05$).

Fig. 3D′). Again, the amplitudes were higher for the FL than HL (peak amplitude HL 0.24% $\Delta f/f_0$ ± 0.02 SEM and FL 0.30% $\Delta f/f_0$ ± 0.03 SEM, $n = 4$, $P < 0.05$, Fig. 3D′). In summary, for all the imaged changes the FL stimulus resulted in a stronger and faster response in the somatosensory cortex compared with the HL stimulation.

To gain a deeper understanding of the somatosensory representations, we characterized the activities in the noncorresponding territories. For instance, we looked at the astrocytic activity in the HL area upon FL stimulation. Stimulation of the forepaw resulted in a much weaker activation in the HL cortex when compared with direct HL stimulation (1.9% $\Delta f/f_0$ ± 0.4 SEM vs. 3.4% $\Delta f/f_0$ ± 0.6 SEM, $P < 0.05$ Fig. 3B′). Similarly, blood flow and neuronal signals were also weaker in the HL area when the noncorresponding limb was stimulated (blood flow: HL stim 6.7% ΔCBF ± 1.1 SEM FL stim 4.1% ΔCBF ± 1.8 SEM, $P < 0.05$; neuronal activity: (VSD imaging) HL stim 0.24% $\Delta f/f_0$ ± 0.02 SEM FL stim 0.05% $\Delta f/f_0$ ± 0.01 SEM, $P < 0.05$ Fig. 3C′,D′). The same was also true for the FL area. Astrocytic activity in this area was just 1.2% $\Delta f/f_0$ ± 0.2 SEM upon hindpaw stimulation compared with 5.4% $\Delta f/f_0$ ± 0.4 SEM upon forepaw stimulation. Blood flow was 2.7% ΔCBF ± 0.7 SEM compared with 14.2% ΔCBF ± 5.5 SEM and neuronal activity was 0.05% $\Delta f/f_0$ ± 0.01 SEM and 0.30% $\Delta f/f_0$ ± 0.03 SEM. In summary, the somatotopic representation of the body in astrocytes is similar to that found in neurons and blood flow activations. Notably, some activity in the noncorresponding area of somatosensory cortex can be driven by the noncorresponding limb but it is significantly weaker than the activity driven by the represented body part.

Neuronal Impact on Astrocytic Activation

Does the astrocytic signal persist even in the absence of local neuronal activity? By applying TTX topically for 60 min, we targetted most of the neurons in the superficial cortical layers. This was confirmed by the absence of evoked neuronal responses from layer 2/3 in both FL and HL sensory areas (Fig. 4A). As stated above, most of the measured astrocytic signals originate from the superficial layers (Fig. 1B). The absence of neuronal activity virtually abolished the astrocytic signals (Fig. 4B). Any reminiscent astrocytic activity

was indistinguishable from noise and without the somatotopic attributes clearly visible before neuronal blockade.

Finally, we addressed how the rate of sensory inputs influences the cortical astrocytic activity. According to previous reports (Norup Nielsen and Lauritzen, 2001) the activation of excitatory neurons and blood flow in the somatosensory cortex is inversely related to the frequency of the stimuli at stimulation frequencies higher than 2 Hz. Correspondingly, the lowest stimulation frequency of 2 Hz showed the strongest responses and the highest frequency of 20 Hz induced the least activity (Fig. 4C). Similarly, astrocytic activity too was dramatically reduced from 3.3% $\Delta f/f_0 \pm 1.0$ SEM at 2 Hz to 1.9% $\Delta f/f_0 \pm 0.6$ SEM at 20 Hz, $n = 4$, $P < 0.05$, Fig. 4D).

DISCUSSION

Using a wide field method to measure astrocytic calcium waves *in vivo*, this study has revealed that cortical astrocytes are recruited somatotopically. We have documented the representation of the rat FL and HL in the contralateral sensory cortex; the neuronal sensory representations of the limbs are juxtapositioned. The astrocytes in the sensory area were strongly driven by the corresponding body part, but stimulation of the noncorresponding part resulted in twofold to fivefold lower responses. The fluorescence indicator Rhod-2 AM reflected the calcium changes and the signal was abolished in the presence of an astrocyte specific tricarboxylic acid cycle blocker. Intriguingly, the neurons remained responsive to sensory inputs in spite of the blocker. In contrast, blocking the neurons in the superficial cortical layers resulted in nonresponsive astrocytes. The neuron–astrocyte interactions revealed here and the astrocytic gap junction networks documented in the literature using diverse methods (Houades et al., 2008; Rouach et al., 2008) converge to predict the somatotopic astrocytic activation in this study.

We have strong arguments and evidence to state that the observed calcium signal changes originated from astrocytes and not neurons. First, the topical application of Rhod-2 AM (the calcium indicator) makes the dye available for uptake to astrocytes but not neurons. The gap junctions between astrocytes spread the indicator to the deeper cell layers. Even in brain slice experiments where the dye is made available to both neurons and astrocytes, only the latter internalize the dye (Mulligan and MacVicar, 2004). Our dye-loading procedure has been used for astrocytic two-photon imaging of the intact rodent brain (Takano et al., 2006). It must be noted here that neurons can be labelled with calcium indicators but only upon injections into the brain (Yaksi and Friedrich, 2006). Second, two-photon imaging revealed Rhod-2-filled star-shaped cells and cells wrapped around blood vessels, and unlabelled cells—presumably neurons. By using genetic tools previous reports have elegantly co-localized Rhod-2-filled cells with an astrocytic marker (Takano et al., 2006). Thirdly and most importantly, the application of FA completely abolished the positive signal in response to sensory stimuli. A relatively small negative component remained. The disappearance of the signal confirms the astrocytes are the source of the positive signal, as FA potently and specifically blocks their metabolic pathways (Fonnum et al., 1997; Swanson and Graham, 1994). The negative component is probably due to uncharacterized intrinsic signals that exist within the wavelengths used to detect Rhod-2 AM. Notably, FA did not abolish the neuronal activity in response to the same stimulations. In fact, the neurons were more responsive to sensory inputs than before the astrocytic block. This excitability can be explained by the diminished clearance of glutamate in the absence of functional astrocytes (Eid et al., 2008). Perhaps when neuronal metabolic and transmitter resources are exhausted they would no longer be able to respond to peripheral sensory inputs. However, our results demonstrate that—in the short term—neurons can elicit bursts of activity in the absence of astrocytic support.

It must be stated here that using FA alone we cannot make strong statements on astrocyte-neuron interactions. The concentration range where the compound is specific for glial cells is narrow and neuronal structures may be directly affected. Moreover, increase of citrate or potassium in the extracellular fluid due to the metabolic block may be toxic to neurons (Largo et al. 1996). In order to circumvent these and similar caveats genetic tools available in mice will come handy. Using these tools astrocyte function can be specifically targeted (Petravicz et al., 2008) or indeed gliotransmission specifically interrupted (Fellin et al., 2009).

In the visual cortex astrocytes are tuned to the orientation of the inputs and in the somatosensory cortex, astrocytes respond to inputs from the body (Wang et al., 2006; Winship et al., 2007; Schummers et al., 2008). Our study examining the FL and HL sensory cortex suggests strong neuron–astrocyte interactions as well. The previous reports focused on a smaller astrocytic population using two-photon imaging, a powerful method for monitoring the activity of individual cells. The method of wide field imaging is well suited to address the spatiotemporal dynamics of astrocytic calcium signals across a large area of the somatosensory cortex. Moreover, this work together with our recent reports using VSDs in the FL and HL sensory cortex allows us to contrast neuronal and astrocytic activations in response to sensory stimulation of the limbs (Ghosh et al., 2009, 2010). Neuronal electrical changes occur within a few ms of stimulus onset and astrocytes take seconds to show calcium signals. Despite the different timescales, the magnitude, the spatial spread and relative timing of the FL and HL activations show notable similarities. The magnitude of FL responses was higher than the HL, in both neurons and astrocytes. Spatially, neuronal HL and FL representations are essentially the same as for astrocytes. For both, the HL is represented caudo-medial to the FL area. A further key temporal pattern is similar for both neurons and astrocytes. Because of the longer distance from the hindpaw to the brain, the evoked HL signals

lag behind FL responses, however, only by 8 ms for neurons but 1.5 s in the case of astrocytes.

In addition to the above mentioned similarities, we also found that blockade of neuronal input abolished astrocytic calcium activity and that with increasing frequency of stimulation both neuronal and astrocytic activities were depressed. Our neuronal measure is biased towards excitatory neurons and presumably the increase in frequency from 2 to 4 Hz recruits inhibitory circuits. Our interpretation is that inhibitory neurons are poor modulators of astrocytic activity, which is compatible with the results from cell culture experiments demonstrating that GABA does not increase astrocytic metabolism (Chatton et al., 2003). The reflection of excitatory neuronal activity in astrocytes must enable the latter cells to replenish neuronal resources in an activity-dependent manner. The mechanisms underlying neuron–astrocyte coupling have recently been reviewed elsewhere (Halassa and Haydon, 2010). It is worth mentioning here that these mechanisms include astrocytic calcium signaling due to released neuronal glutamate. Moreover, our findings are notably distinct from the large-scale calcium waves ("glissandi") recently discovered in the hippocampus (Kuga et al., 2011).

It is commonly held that astrocytes are functionally connected via gap junctions (Verkhratsky and Kettenmann, 1996; Giaume et al., 2010). How is the astrocytic activity largely restricted to the HL or FL sensory cortex? Anatomically, the astrocytes serving the same whisker barrel in the somatosensory cortex are densely connected than across barrels (Houades et al., 2008). Similarly, the astrocytes in the FL and HL cortices may be anatomically configured to interact more intensely within than across the areas. In our study, a vivid violation of this anatomical restriction occurred along the pial veins. Strong signals were observed there across the FL and HL fields. The significance and underlying mechanisms of these signals will be systematically addressed in subsequent reports. Astrocytes in proximity to the veins, sub-pial astrocytic sheaths, glial limitans or even venous endothelial cells may all directly or indirectly contribute to the signal (Arcuino et al., 2002; McCaslin et al., 2011). Furthermore, a peripheral signal could be another potential source of the activation along the surface veins. But, the later seems less likely as the calcium signals disappear with the suppression of local neuronal activity.

In this discussion, we focused on the neuron–astrocyte interactions more than on the hemodynamic aspects. Several studies have shown that astrocytes mediate CBF (Zonta et al., 2003; Takano et al., 2006; Gordon et al., 2008). In our report, it is apparent that the changes in blood flow proceed astrocytic (bulk) activity. But, our method is presumably insensitive to the short-latency calcium signals that play a crucial role in regulating hemodynamics (Winship et al., 2007). One reason for this insensitivity must be due to the small fraction (~5%) of astrocytes that respond with short latencies. In addition, astrocytic calcium increases at the endfeet—which are related to vascular dilation (Petzold et al., 2008)—may only marginally contribute to the signal dominated by a larger calcium rich somatic component. Presumably, the astrocytic signal reported in our study is involved in sustaining altered hemodynamics (Schulz et al., 2012).

In conclusion, the astrocytic maps revealed here have direct implications on how neuronal functions are regulated. For instance, as astrocytes influence neuronal NMDA receptors, such influences must be restricted to brain areas with strong astrocytic links (Halassa and Haydon, 2010). However, the prolonged activation of astrocytes may allow for the integration of sensory information over several seconds. It is hoped that this study will stimulate new lines of investigation on how the astrocytic maps are developed and maintained in health and contribute to disease.

ACKNOWLEDGMENTS

The authors thank Prof. Martin Schwab and Prof. Kevan Martin for their crucial guidance in the pilot phase of this study and Dr. Bjorn Kampa for his help with the two-photon imaging.

REFERENCES

Aguado F, Espinosa-Parrilla JF, Carmona MA, Soriano E. 2002. Neuronal activity regulates correlated network properties of spontaneous calcium transients in astrocytes in situ. J Neurosci 22:9430–9444.

Araque A, Navarrete M. 2010. Glial cells in neuronal network function. Philos Trans R Soc Lond B Biol Sci 365:2375–2381.

Arcuino G, Lin JH, Takano T, Liu C, Jiang L, Gao Q, Kang J, Nedergaard M. 2002. Intercellular calcium signaling mediated by point-source burst release of ATP. Proc Natl Acad Sci USA 99:9840–9845.

Bonvento G, Charbonne R, Correze JL, Borredon J, Seylaz J, Lacombe P. 1994. Is alpha-chloralose plus halothane induction a suitable anesthetic regimen for cerebrovascular research? Brain Res 665:213–221.

Chatton JY, Pellerin L, Magistretti PJ. 2003. GABA uptake into astrocytes is not associated with significant metabolic cost: Implications for brain imaging of inhibitory transmission. Proc Natl Acad Sci USA 100:12456–12461.

Cornell-Bell AH, Finkbeiner SM. 1991. Ca2+ waves in astrocytes. Cell calcium 12:185–204.

Dunn AK, Devor A, Dale AM, Boas DA. 2005. Spatial extent of oxygen metabolism and hemodynamic changes during functional activation of the rat somatosensory cortex. Neuroimage 27:279–290.

Eid T, Ghosh A, Wang Y, Beckstrom H, Zaveri HP, Lee TS, Lai JC, Malthankar-Phatak GH, de Lanerolle NC. 2008. Recurrent seizures and brain pathology after inhibition of glutamine synthetase in the hippocampus in rats. Brain 131(Pt 8):2061–2070.

Fellin T, Halassa MM, Terunuma M, Succol F, Takano H, Frank M, Moss SJ, Haydon PG. 2009. Endogenous nonneuronal modulators of synaptic transmission control cortical slow oscillations in vivo. Proc Natl Acad Sci USA 106:15037–15042.

Fonnum F, Johnsen A, Hassel B. 1997. Use of fluorocitrate and fluoroacetate in the study of brain metabolism. Glia 21:106–113.

Francis JT, Xu S, Chapin JK. 2008. Proprioceptive and cutaneous representations in the rat ventral posterolateral thalamus. J Neurophysiol 99:2291–2304.

Ghosh A, Haiss F, Sydekum E, Schneider R, Gullo M, Wyss MT, Mueggler T, Baltes C, Rudin M, Weber B, Schwab ME. 2010. Rewiring of hindlimb corticospinal neurons after spinal cord injury. Nat Neurosci 13:97–104.

Ghosh A, Sydekum E, Haiss F, Peduzzi S, Zorner B, Schneider R, Baltes C, Rudin M, Weber B, Schwab ME. 2009. Functional and anatomical reorganization of the sensory-motor cortex after incomplete spinal cord injury in adult rats. J Neurosci 29:12210–12219.

Giaume C, Koulakoff A, Roux L, Holcman D, Rouach N. 2010. Astroglial networks: a step further in neuroglial and gliovascular interactions. Nat Rev Neurosci 11:87–99.
Gochin PM, Bedenbaugh P, Gelfand JJ, Gross CG, Gerstein GL. 1992. Intrinsic signal optical imaging in the forepaw area of rat somatosensory cortex. Proc Nat Acad Sci USA 89:8381–8383.
Gordon GR, Choi HB, Rungta RL, Ellis-Davies GC, MacVicar BA. 2008. Brain metabolism dictates the polarity of astrocyte control over arterioles. Nature 456:745–749.
Halassa MM, Haydon PG. 2010. Integrated brain circuits: Astrocytic networks modulate neuronal activity and behavior. Annu Rev Physiol 72:335–355.
Houades V, Koulakoff A, Ezan P, Seif I, Giaume C. 2008. Gap junction-mediated astrocytic networks in the mouse barrel cortex. J Neurosci 28:5207–5217.
Iadecola C, Nedergaard M. 2007. Glial regulation of the cerebral microvasculature. Nat Neurosci 10:1369–1376.
Kozlov AS, Angulo MC, Audinat E, Charpak S. 2006. Target cell-specific modulation of neuronal activity by astrocytes. Proc Natl Acad Sci USA 103:10058–10063.
Kuga N, Sasaki T, Takahara Y, Matsuki N, Ikegaya Y. 2011. Large-scale calcium waves traveling through astrocytic networks in vivo. J Neurosci 31:2607–2614.
Langer D, van't Hoff M, Helmchen F. 2010. Helioscan, a highly versatile control software for laser-scanning microscopes written in LabVIEW. Switzerland: Brain Research Institute, University of Zurich.
Largo C, Cuevas P, Somjen GG, Martin del Rio R, Herreras O. 1996. The effect of depressing glial function in rat brain in situ on ion homeostasis, synaptic transmission, and neuron survival. J Neurosci 16:1219–1229.
McCaslin AF, Chen BR, Radosevich AJ, Cauli B, Hillman EM. 2011. In vivo 3D morphology of astrocyte-vasculature interactions in the somatosensory cortex: Implications for neurovascular coupling. J Cereb Blood Flow Metabol 31:795–806.
Mothet JP, Pollegioni L, Ouanounou G, Martineau M, Fossier P, Baux G. 2005. Glutamate receptor activation triggers a calcium-dependent and SNARE protein-dependent release of the gliotransmitter D-serine. Proc Natl Acad Sci USA 102:5606–5611.
Mulligan SJ, MacVicar BA. 2004. Calcium transients in astrocyte endfeet cause cerebrovascular constrictions. Nature 431:195–199.
Navarrete M, Perea G, Maglio L, Pastor J, Garcia de Sola R, Araque A. in press. Astrocyte calcium signal and gliotransmission in human brain tissue. Cereb Cortex.
Nett WJ, Oloff SH, McCarthy KD. 2002. Hippocampal astrocytes in situ exhibit calcium oscillations that occur independent of neuronal activity. J Neurophysiol 87:528–537.
Norup Nielsen A, Lauritzen M. 2001. Coupling and uncoupling of activity-dependent increases of neuronal activity and blood flow in rat somatosensory cortex. J Physiol 533(Pt 3):773–785.
Pascual O, Casper KB, Kubera C, Zhang J, Revilla-Sanchez R, Sul JY, Takano H, Moss SJ, McCarthy K, Haydon PG. 2005. Astrocytic purinergic signaling coordinates synaptic networks. Science 310:113–116.
Paxinos G, Watson C. 2006. The rat brain in stereotaxic coordinates. San Diego: Academic Press.
Pellerin L, Magistretti PJ. 1994. Glutamate uptake into astrocytes stimulates aerobic glycolysis: A mechanism coupling neuronal activity to glucose utilization. Proc Natl Acad Sci USA 91:10625–10629.
Perea G, Araque A. 2007. Astrocytes potentiate transmitter release at single hippocampal synapses. Science 317:1083–1086.
Petravicz J, Fiacco TA, McCarthy KD. 2008. Loss of IP3 receptor-dependent Ca2+ increases in hippocampal astrocytes does not affect baseline CA1 pyramidal neuron synaptic activity. J Neurosci 28:4967–4973.
Petzold GC, Albeanu DF, Sato TF, Murthy VN. 2008. Coupling of neural activity to blood flow in olfactory glomeruli is mediated by astrocytic pathways. Neuron 58:897–910.
Rouach N, Koulakoff A, Abudara V, Willecke K, Giaume C. 2008. Astroglial metabolic networks sustain hippocampal synaptic transmission. Science 322:1551–1555.
Schulz K, Sydekum E, Krueppel R, Engelbrecht CJ, Schlegel F, Schroter A, Rudin M, Helmchen F. 2012. Simultaneous BOLD fMRI and fiber-optic calcium recording in rat neocortex. Nature methods 9:597–602.
Schummers J, Yu H, Sur M. 2008. Tuned responses of astrocytes and their influence on hemodynamic signals in the visual cortex. Science 320:1638–1643.
Swanson RA, Graham SH. 1994. Fluorocitrate and fluoroacetate effects on astrocyte metabolism in vitro. Brain Res 664:94–100.
Sydekum E, Baltes C, Ghosh A, Mueggler T, Schwab ME, Rudin M. 2009. Functional reorganization in rat somatosensory cortex assessed by fMRI: Elastic image registration based on structural landmarks in fMRI images and application to spinal cord injured rats. Neuroimage 44:1345–1354.
Takano T, Tian GF, Peng W, Lou N, Libionka W, Han X, Nedergaard M. 2006. Astrocyte-mediated control of cerebral blood flow. Nat Neurosci 9:260–267.
Verkhratsky A, Kettenmann H. 1996. Calcium signalling in glial cells. Trends Neurosci 19:346–352.
Wang X, Lou N, Xu Q, Tian GF, Peng WG, Han X, Kang J, Takano T, Nedergaard M. 2006. Astrocytic Ca2+ signaling evoked by sensory stimulation in vivo. Nat Neurosci 9:816–823.
Winship IR, Plaa N, Murphy TH. 2007. Rapid astrocyte calcium signals correlate with neuronal activity and onset of the hemodynamic response in vivo. J Neurosci 27:6268–6272.
Yaksi E, Friedrich RW. 2006. Reconstruction of firing rate changes across neuronal populations by temporally deconvolved Ca2+ imaging. Nat Methods 3:377–383.
Zakharov P, Volker AC, Wyss MT, Haiss F, Calcinaghi N, Zunzunegui C, Buck A, Scheffold F, Weber B. 2009. Dynamic laser speckle imaging of cerebral blood flow. Opt Express 17:13904–13917.
Zilles K, Zilles B, Schleicher A. 1980. A quantitative approach to cytoarchitectonics. VI. The areal pattern of the cortex of the albino rat. Anat Embryol 159:335–360.
Zonta M, Angulo MC, Gobbo S, Rosengarten B, Hossmann KA, Pozzan T, Carmignoto G. 2003. Neuron-to-astrocyte signaling is central to the dynamic control of brain microcirculation. Nat Neurosci 6:43–50.